LANGMUIR

pubs.acs.org/Langmuir Article

Controlled Temporal Release of Serum Albumin Immobilized on Gold Nanoparticles

Tosin Ogunlusi and Jeremy D. Driskell*

Cite This: *Langmuir* 2023, 39, 3720−3728 Read Online

ACCESS | Metrics & More | Article Recommendations | Supporting Information

ABSTRACT: Proteins adsorbed to gold nanoparticles (AuNPs) form bioconjugates and are critical to many emerging technologies for drug delivery, diagnostics, therapies, and other biomedical applications. A thorough understanding of the interaction between the immobilized protein and AuNP is essential for the bioconjugate to perform as designed. Here, we explore a correlation between the number of solvent-accessible thiol groups on a protein and the protein desorption rate from the AuNP surface in the presence of a competing protein. The chemical modification of human serum albumin (HSA) was carried out to install additional free thiols using Traut's reagent and create a library of HSA analogues by tailoring the molar excess of the Traut's reagent. We pre-adsorbed HSA variants onto the AuNP surface, and the resulting bioconjugates were then exposed to IgG antibody, and protein exchange was monitored as a function of time. We found that the rate of HSA displacement from the AuNP correlated with the experimentally measured number of accessible free thiol groups. Additionally, bioconjugates were synthesized using thiolated analogues of bovine serum albumin (BSA) and suspended in serum as a model for a complex sample matrix. Similarly, desorption rates with serum proteins were modulated with solvent-accessible thiols on the immobilized protein. These results further highlight the key role of Au−S bonds in the formation of protein−AuNP conjugates and provide a pathway to systematically control the number of free thiols on a protein, enabling the controlled release of protein from the surface of AuNP.

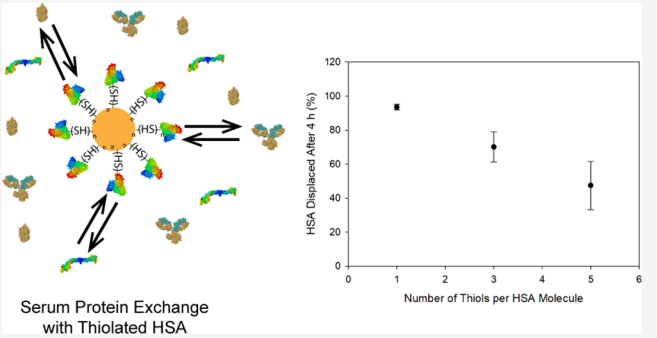

INTRODUCTION

Advanced delivery systems for therapeutic proteins offer the promise of targeted delivery and sustained or stimulated release to reduce adverse side effects and enhance efficacy.[1,2] Several nanomaterials have been explored as delivery platforms due to high drug loading capacity and tunable properties to potentially regulate the release rate of protein drugs. For example, temperature-responsive polymers and cross-linking density have been leveraged to trigger or slow the release rate of drug molecules loaded in polymeric hydrogels.[3,4] Electrostatic forces between a protein and mesoporous silica can be regulated by pH to influence desorption.[5] Laponite nanoplatelets with electrolytes facilitate the adsorption/desorption of therapeutic proteins via electrostatic control, and when loaded in a hydrogel or cryogel, have been demonstrated to slow the release of biofunctional proteins.[6−8] Many of these novel approaches rely on direct but nonspecific interactions between therapeutic proteins and the nanomaterial for delivery.[9−12] Of particular interest is the systematic control of the interaction between the therapeutic protein and nanomaterial to modulate the protein release profile as needed. Thus, to realize the potential of these innovative systems, a thorough understanding of the interaction between the protein and the delivery vehicle is required.

Gold nanoparticles (AuNPs) are one of the many nanometric drug carriers currently being investigated.[13−15] AuNPs are readily synthesized with a variety of morphologies and surface chemistries and are biocompatible. In addition, the plasmonic property of AuNPs affords localized heating for triggered drug release or enables simultaneous diagnostic capabilities that have led to emerging theranostics.[16−18] With the promise of these potential benefits in drug delivery and other biomedical applications,[19−25] protein−AuNP interactions have been the focus of many recent studies. Previous works have identified many contributing factors responsible for the adsorption of proteins onto the surface of AuNPs, including electrostatic forces, hydrophobic interactions, and Au−S chemisorption; however, Au−S chemisorption has been recognized as the dominant mechanism by which proteins bind to AuNPs.[26−31] Those past works primarily focused on

Received: December 22, 2022
Revised: January 31, 2023
Published: March 1, 2023

interactions under equilibrium conditions, where the objective was to understand and maximize the protein−AuNP binding affinity to form a robust and stable conjugate. Here, we postulate that those mechanistic insights provide an opportunity to modulate protein−AuNP interaction to control the desorption rate when in the presence of competing proteins.

Previously in our lab, we demonstrated that thiols control the final protein corona composition.[27,32] Specifically, IgG displays 10 solvent-accessible sulfur atoms and displaces human serum albumin (HSA), which possesses one free thiol. However, HSA chemically modified with 20 thiols resisted displacement by IgG molecules.[32] Thus, that foundational work identified solvent-accessible thiols as one parameter to form stable conjugates. Here, we investigate HSA and HSA analogues that will be displaced by IgG in serum but give particular attention to the rate at which protein exchange occurs. In this study, Traut's reagent, a chemical modifier, was used to install solvent-accessible thiols on HSA as a primary factor to manipulate the interaction between the protein and AuNPs. Several thiolated analogues of HSA were synthesized, and the desorption rates of the proteins from the surface of AuNP were measured when the conjugates were exposed to a competing protein to test a hypothesized correlation between protein thiolation and desorption rate.

HSA by itself is not a therapeutic protein; however, several small molecule drugs have been complexed with HSA to function as therapeutic agents.[33−35] Conjugation of small drug molecules to HSA can extend drug half-life and enhance drug accumulation in tumor tissues; thus, the outcomes of this work are directly relevant to HSA-small drug molecule conjugates using AuNP as a nanocarrier. More generally, HSA serves as a model system, and the insights gained herein can be leveraged for AuNP delivery of other therapeutic proteins.

EXPERIMENTAL SECTION

Materials and Reagents. Citrate-capped, spherical AuNPs with a nominal diameter of 60 nm and concentration of 2.6×10^{10} AuNP/mL were purchased from Ted Pella Inc. (Redding, CA). Anti-horseradish peroxidase monoclonal antibody (anti-HRP, 4.4 mg/mL) and normal bovine serum were obtained from My BioSource. Fluorescein isothiocyanate-labeled bovine serum albumin (FITC BSA) and human serum albumin (HSA) were obtained from Sigma-Aldrich (St. Louis, MO). Horseradish peroxidase (HRP), 2,2′-azino-bis (3-ethylbenzothiazoline-6-sulfonic acid) (1-Step ABTS), 5,5′-dithio-bis (2-nitrobenzoic acid) (Ellman's reagent), and 2-iminothiolane (Traut's reagent) were purchased from Thermo Scientific (Rockford, IL). Potassium phosphate monohydrate and potassium cyanide were acquired from Fisher Scientific (Fair Lawn, NJ). Anhydrous potassium phosphate dibasic was purchased from Mallinckrodt Chemicals, Inc. (Paris, KY). A Barnstead water purification system (Thermo Scientific, Rockford, IL) provided nanopure deionized water (18 MΩ) and was used in the preparation of all aqueous solutions.

Chemical Modification of Protein with Traut's Reagent. Several thiolated species of HSA were synthesized by reacting HSA with a freshly prepared solution of Traut's reagent. Traut's reagent was added to HSA (60 μM) in molar excesses of 7-fold, 20-fold, 25-fold, and 30-fold, gently mixed on a shaker, and allowed to react for 60 min at room temperature. After incubation, the chemically modified HSA (T-HSA) analogues were purified using a Zeba spin desalting column (7 kDa MWCO, Thermo Scientific) to remove excess, unreacted Traut's reagent. Following the manufacturer's protocol, the column was centrifuged at 1500*g* for 1 min to remove the initial storage solution. Thereafter, 300 μL of phosphate buffer (2 mM, pH 8.0) was added to the spin column and centrifuged at 1500*g* for 1 min to equilibrate the column resin. This procedure was repeated three times, with the buffer being discarded after each wash. The T-HSA reaction mixture (105 μL) was added to the column and centrifuged at 1500*g* for 2 min in a clean centrifuge tube to collect the purified T-HSA solution. After the protein purification process, the final concentration of T-HSA was determined using a Nanodrop 2000 (Thermo Scientific) and the extinction coefficient for BSA (43,824 M^{-1} cm^{-1}) that is preprogrammed in the instrument software. Fluorescently labeled BSA (FITC BSA) was modified with Traut's reagent following the same protocol to synthesize FITC T-BSA analogues.

Determination of Free Thiols with Ellman's Reagent. Ellman's reagent (5,5-dithio-bis-[2-nitrobenzoic acid]) was used to quantify the free thiol groups present in each HSA analogue using cysteine as a thiol-containing external standard. A solution of Ellman's reagent was prepared at 4 mg/mL phosphate buffer (0.1 M, pH 8.0, with 1 mM EDTA). Calibration standards of cysteine ranging from 0−1000 μM were prepared by serial dilution. Protein samples, i.e., HSA analogues, were prepared at 4 mg/mL (60.6 μM). In triplicate, 46.5 μL of 2 mM phosphate buffer, 3.5 μL of freshly prepared Ellman's reagent, and 10 μL of standard or sample were mixed in wells of a 96-well plate. The resulting mixture was incubated for 30 min, and the absorbance of each well was measured at 415 nm with a microplate reader. A calibration curve was plotted and used to quantify free thiols presented by the HSA analogues. The same approach was used to determine free thiols that are present in a fluorescently labeled protein (FITC BSA).

Protein−AuNP Conjugate Formation. The protein−AuNP bioconjugates were synthesized by adding AuNPs (60 nm, 100 μL) to a low binding microcentrifuge tube, followed by centrifugation at 5000*g* for 5 min. The supernatant was discarded. A solution of HSA or T-HSA (100 μL, 4 mg/mL) was added to the pelleted AuNP and gently mixed to resuspend the colloid. The protein−AuNP mixture was incubated for 1 h at room temperature with gentle shaking to ensure thorough mixing. After incubation, the AuNP suspension was centrifuged at 5000*g* for 5 min and the supernatant was discarded to remove excess protein. The protein−AuNP conjugate was then resuspended in 2 mM phosphate buffer (pH 8.0) and centrifuged/resuspended three additional times for the thorough removal of excess protein.

Quantifying Protein Displacement from the Surface of AuNPs. *Enzyme-Based Assay to Quantify Protein Displacement.* Using a previously described approach in our group,[32] we investigated the displacement of the preadsorbed protein from the AuNP surface caused by the introduction of competing proteins to the protein−AuNP bioconjugate. Briefly, HSA (4 mg/mL) or T-HSA (4 mg/mL) was immobilized on AuNPs and incubated for 1 h to form a hard corona. Purification of the HSA- or T-HSA-AuNP bioconjugate was carried out via three centrifugation/resuspension cycles. An anti-HRP antibody (3 μL, 1 mg/mL) was introduced to the suspension of the purified HSA- or T-HSA-AuNPs bioconjugate and thoroughly mixed. Protein exchange was allowed to take place for 1, 4, 9, 12, 48, and 72 h on the AuNP surface. Thereafter, the bioconjugates were centrifuged at 5000*g* for 5 min, and the supernatant was discarded to remove any unbound or displaced proteins. Next, the bioconjugates were resuspended in 2 mM phosphate buffer (pH 8.0), and three additional centrifugation cycles were performed for the thorough removal of excess protein from the bioconjugates.

An enzymatic assay was performed to determine an anti-HRP antibody loading on the conjugates and to quantify the extent to which HSA or T-HSA was displaced by the anti-HRP antibody. The purified protein−AuNP bioconjugate suspensions were incubated with excess HRP (3 μL, 1 mg/mL) for 1 h to saturate the available antigen-binding sites of the anti-HRP antibody immobilized on the AuNP bioconjugate. Excess HRP was then removed from the conjugates via four centrifugation cycles. Next, 10 μL of the conjugate was mixed with 150 μL of 1-Step ABTS (2,2′-azino-bis-[3-ethylbenzothiazoline-6-sulfonic acid]) solution in a 96-well plate. The absorbance at 415 nm was measured at 10 s intervals for 20 min using a microplate reader to monitor the formation of the enzyme-catalyzed product. The reaction rate was normalized to the

https://doi.org/10.1021/acs.langmuir.2c03429
Langmuir 2023, 39, 3720−3728

concentration of bioconjugates measured with inductively coupled plasma-optical emission spectroscopy (ICP-OES).

Fluorescence-Based Assay to Quantify Protein Displacement. FITC BSA was dissolved in 2 mM phosphate buffer (pH 8.0) and then adsorbed onto the surface of AuNPs to form a bioconjugate. A 100 μL of 60 nm AuNPs was placed in a low binding microcentrifuge tube, followed by centrifugation at 5000*g* for 5 min. The supernatant was discarded. FITC BSA or Traut's reagent-modified FITC BSA (100 μL, 4 mg/mL) was added to the sedimented AuNP pellet, the AuNP was re-dispersed, and the mixture was allowed to incubate for 1 h. After incubation, the AuNP suspension was centrifuged at 5000*g* for 5 min to remove excess protein. Protein−AuNP conjugate was then resuspended in 2 mM phosphate buffer (pH 8.0) and centrifuged three additional times for the thorough removal of excess protein. Next, 10% normal bovine serum was introduced to the suspension of the purified FITC BSA or FITC T-BSA bioconjugate and gently mixed on a shaker. Protein displacement was allowed to take place for 1 h on the AuNP surface. After the incubation, the bioconjugates were centrifuged at 5000*g* for 5 min and the supernatant was collected to quantify the displaced FITC BSA or FITC T-BSA via fluorescence.

Characterization of Proteins and Bioconjugates. *Quantitation of Protein−AuNP Bioconjugates Using ICP-OES.* ICP-OES was used to analyze the concentration of bioconjugates. To accomplish this, 50 μL of the bioconjugate was loaded into a low binding tube, and 5 μL of 100 mM potassium cyanide was added for the complete dissolution of AuNPs. After dissolution, the clear solution was diluted to a final volume of 5.00 mL with 2% nitric acid. Calibration standards were prepared in 2% nitric acid with Au concentrations ranging from 0.1 to 10 ppm. ICP-OES was used to analyze the prepared samples and Au calibration standards. The samples were introduced at 1 mL/min into the plasma operating at 1500 W, and the emission intensity at 242.795 nm was integrated for 15 s.

Dynamic Light Scattering. A Malvern Zetasizer Nano ZSP was employed for the analysis of the mean hydrodynamic diameter of HSA, T-HSA, unconjugated AuNP, and protein−AuNP bioconjugates. Eighty microliters of sample was carefully added to a microvolume cuvette, which was interrogated by the laser. Dynamic light scattering (DLS) was carried out to determine the hydrodynamic diameter of the proteins and bioconjugates using the cumulants method (z-average), and the size measurement was performed in triplicate, where each measurement is the average of 15 separate 10 s runs.

UV−Visible Spectrophotometry. UV−visible measurements were carried out using an Agilent 8453 spectrophotometer (Santa Clara, CA) operating from 190 to 1100 nm to measure the concentration of protein and evaluate the conjugation of protein to AuNP. A Viroskan LUX multimode microplate reader (ThermoFisher Scientific) was used to measure the absorbance of products formed in the enzyme assays conducted in 96-well plates.

Fluorescence Spectroscopy. Fluorescence spectra were acquired using a Cary Eclipse fluorescence spectrometer from Agilent. Samples were excited at 495 nm, and emission was measured at 520 nm as recommended by the manufacturer's protocol for albumin−fluorescence isothiocyanate conjugate. Spectra were collected with 10 s integration, and the excitation/emission slit widths of 5/5 nm were used for optimal signal-to-noise ratio.

Circular Dichroism. Circular dichroism spectra were acquired with a Jasco J-1100 spectrophotometer. Samples were prepared at 0.1 mg/mL and loaded into a quartz cuvette with a 0.1 mm path length. Spectra were acquired at 20 °C over the range of 190−260 nm. The secondary structure of protein samples was estimated using the available online software BeStSel.[36,37]

RESULTS AND DISCUSSION

Chemical Modification and Characterization of HSA. Our previous work demonstrated that the number of free thiols presented by the protein controls the stability and robustness of the protein−AuNP interaction.[27,32] We installed additional thiol functional groups on proteins to afford a strong/irreversible interaction between the protein and AuNP. In this work, our goal was to systematically control the number of thiols to facilitate controlled protein desorption. The chemical modification of the surface-accessible lysine residues on human serum albumin (HSA) was carried out using Traut's reagent (2-iminothiolane). Traut's reagent covalently bonded to primary amines of lysine residue to introduce high-affinity thiol groups during modification. Traut's reagent was selected as a chemical modifier because it maintains the same charge as lysine that could impact protein folding/function, adsorption kinetics, immobilized orientation, and affinity of HSA-AuNP binding.[28,38,39] A library of HSA variants was synthesized by controlling the molar excess of the Traut's reagent to vary the number of thiols (Table 1).

Table 1. HSA Modification Conditions and Resulting Analogues

description	molar excess of Traut's reagent	free thiols per protein
HSA		1.1 ± 0.1
3T-HSA	7	2.62 ± 0.04
5T-HSA	20	5.15 ± 0.04
10T-HSA	25	9.9 ± 0.2
14T-HSA	30	13.8 ± 0.1

Chemical modification of HSA was confirmed by quantifying the number of thiol groups using Ellman's reagent. A calibration curve was generated from cysteine standard solutions and established a linear relationship between the concentration of accessible free thiols and the measured TNB product (Figure S1). The number of free thiols per protein was calculated as the ratio of free thiol molar concentration to protein molar concentration (Table 1). We measured approximately one free thiol in unmodified HSA using Ellman's reagent, which agrees with bioinformatics database[40] and molecular dynamic studies using UCSF chimera.[41] Increasing the molar excess of Traut's reagent that reacted with HSA yielded T-HSA analogues with approximately 3, 5, 10, and 14 free thiols per protein molecule (Table 1), and these analogues are referred to as 3T-HSA, 5T-HSA, 10T-HSA, and 14T-HSA, respectively.

HSA and thiolated HSA were further characterized to confirm that chemical modification of HSA with Traut's reagent did not cause conformational changes in the HSA structure, induce protein unfolding, or result in intermolecular cross-linking via disulfide bonds. The most heavily modified analogue, e.g., 14T-HSA, was characterized and compared to the native HSA molecule. The secondary structures of HSA and 14T-HSA were interrogated via circular dichroism (Figure 1). The CD spectrum is unchanged for the thiolated HSA, and further curve-fitting analysis identified 75 and 73% α-helices, 2.8 and 2.3% antiparallel, and 4.0 and 4.0% parallel β-sheets for HSA and 14T-HSA, respectively, establishing that chemical modification did not cause conformational changes.[36,37] The hydrodynamic diameters of native HSA and 14T-HSA measured 8.0 and 7.9 nm, respectively, by DLS (Figure 2). These data are in agreement with the known size of HSA (8 nm × 3 nm)[42] and previously measured hydrodynamic diameters of HSA,[32,39] confirming that the thiolated protein was stable in solution and did not aggregate via intermolecular disulfide bridging.

Adsorption of HSA and 14T-HSA onto Gold Nanoparticles. AuNPs were mixed with 60 μM HSA or 14T-HSA

https://doi.org/10.1021/acs.langmuir.2c03429
Langmuir 2023, 39, 3720−3728

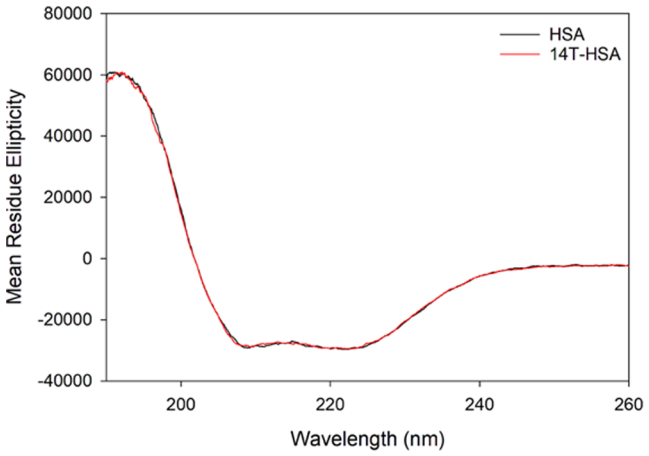

Figure 1. CD spectra of unmodified HSA and thiolated 14T-HSA.

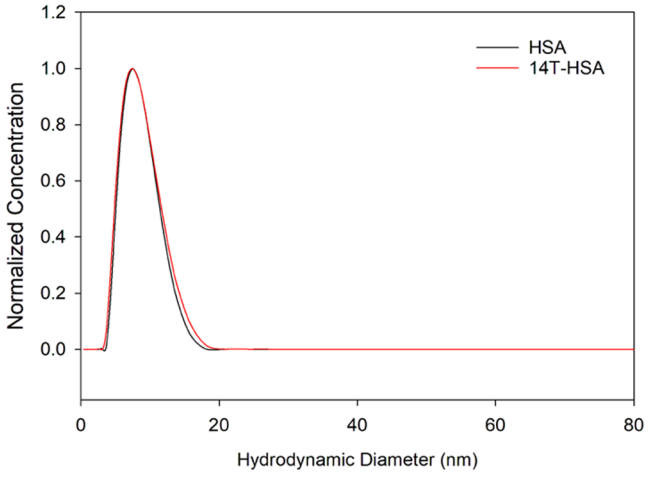

Figure 2. Hydrodynamic diameter size distribution curve of HSA and 14T-HSA measured with DLS.

to allow for passive adsorption of protein onto the surface of AuNPs to form bioconjugates.[27,43−46] The protein concentration was in large excess to allow for monolayer coverage and the possibility of protein multilayers. After the removal of the excess, unbound protein, the purified bioconjugates were characterized with UV−visible spectrophotometry to assess the adsorbed protein layer on the surface of the AuNP. The unconjugated AuNP presented an extinction maximum at 536 nm, and the conjugates formed with native HSA and 14T-HSA exhibited a 2 nm red shift relative to the unconjugated AuNP (Figure 3). This red shift reflects a change in the local refractive index at the surface of the AuNP and indicates the adsorption of protein onto the surface of AuNP.[47] The equivalent shift in the extinction band for both bioconjugates suggests that HSA and 14T-HSA form monolayers on the AuNP. The hydrodynamic diameters of the conjugates were then measured and compared to the unconjugated AuNP to further confirm the adsorption of the protein layer. Figure 3B shows similar hydrodynamic diameters for conjugates formed with HSA and 14T-HSA and represent an increase of ∼8 nm relative to the unconjugated AuNP that results from the adsorbed protein layer. The expected increase in diameter resulting from the adsorbed protein layer is 6−16 nm based on the dimension of the HSA protein. The observed ∼8 nm increase in size is characteristic of a specific molecular orientation upon adsorption and is consistent with previous work detailing the orientation of adsorbed HSA.[39]

The adsorption behavior of HSA and 14T-HSA was investigated to further corroborate the installation of thiols onto HSA via chemical modification with Traut's reagent. Increasing concentrations of HSA and 14T-HSA were added to AuNPs, and the hydrodynamic diameter of the formed conjugates was measured by DLS. For both proteins, the mean hydrodynamic diameter increased with a corresponding increase in protein concentration before reaching a maximum size at monolayer coverage (Figure 4). The adsorption isotherms are best-fit to the Hill-modified Langmuir equation, and the binding parameters extracted from the fit are summarized in Table 2.[48−53] Notably, the thiolated HSA exhibits a greater binding affinity (K_d = 350 ± 60 nM) than the native HSA (K_d = 1833 ± 443 nM). The measured K_d value for HSA is consistent with previously reported values,[54] and the increase in adsorption affinity for the 14T-HSA analogue is anticipated due to the additional high-affinity free thiol functional groups.[26,28−30,38,55] Additionally, the thickness of the protein layer at saturating coverage is equivalent for the

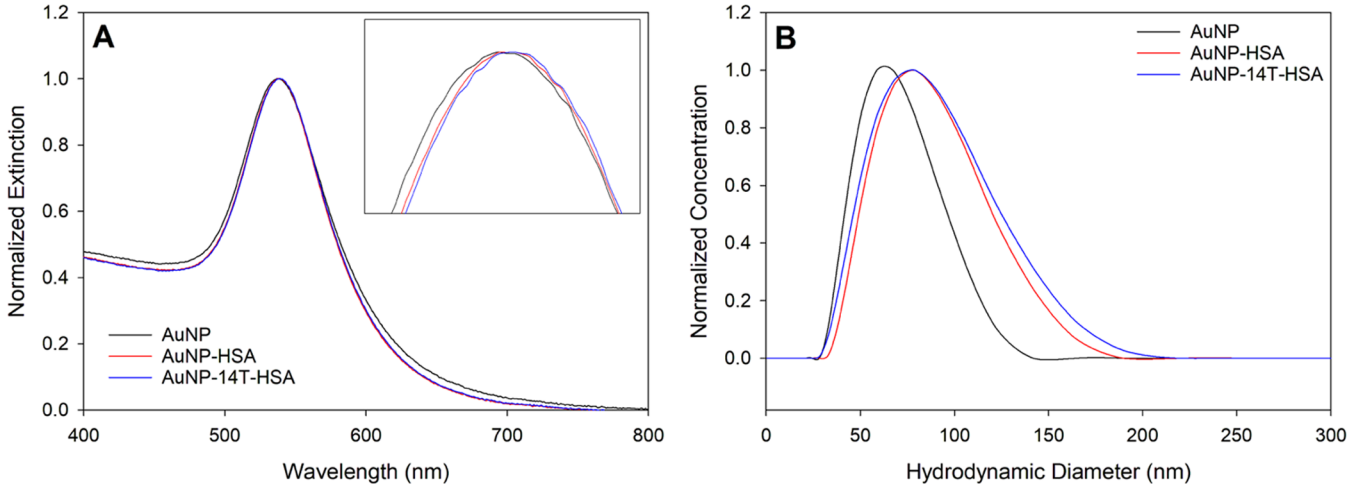

Figure 3. Characterization of protein−AuNP bioconjugates. Representative UV−visible extinction spectra (A) and DLS size distribution curves (B) of unconjugated AuNP, HSA-AuNP conjugates, and 14T-HSA-AuNP conjugates.

https://doi.org/10.1021/acs.langmuir.2c03429
Langmuir 2023, 39, 3720−3728

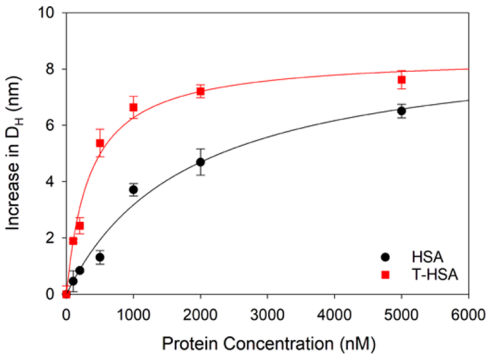

Figure 4. Adsorption isotherms of HSA (black circles) and T-HSA (red squares) binding to AuNP. Protein binding is determined by an increase in the hydrodynamic diameter (D_H) relative to unconjugated AuNPs measured by DLS.

Table 2. Protein Adsorption Parameters Determined from Best-Fit of DLS Adsorption Isotherm (Figure 4) to the Hill−Langmuir Model

protein	K_d (nM)	$\Delta D_{H,max}$ (nm)	R^2
HSA	1833 ± 443	9.0 ± 1.0	0.9817
14T-HSA	350 ± 60	8.4 ± 0.4	0.9852

proteins ($\Delta D_{H,max}$ = 9.0 ± 1.0 nm for HSA and $\Delta D_{H,max}$ = 8.4 ± 0.4 nm for 14T-HSA), indicating that both proteins adsorb to form monolayers and intermolecular disulfide bridges are not formed with the 14T-HSA analogue.

Rate of Protein Displacement. *HSA Displacement from AuNP by IgG.* Previous works suggest the number of solvent-accessible thiols dictates protein corona formed around gold nanoparticles. For example, wild-type GB3, a protein without cysteine residues, pre-adsorbed on a gold nanoparticle was readily displaced by a small organothiol molecular probe, yet a thiolated mutant of GB3 adsorbed onto a gold nanoparticle surface-resisted displacement by the same organothiol molecule.[28] In another example, an IgG molecule with 10 accessible thiol functional groups outcompeted other plasma proteins with fewer cysteine residues, such as HSA, fibrinogen, and transferrin, for adsorption sites on AuNP.[27] More recently, chemical modification of HSA to install a defined number of thiols established a correlation between the composition of the adsorbed protein corona and the number of thiols presented by each protein.[32] Much of the previous work on protein exchange and protein corona formation has focused on the protein adlayer composition under equilibrium conditions. In this work, we explore the possibility of exploiting the number of accessible thiols on a protein to control the rate of protein exchange, e.g., desorption.

Our lab recently developed a quantitative method to measure protein exchange on the surface of AuNPs using an anti-HRP antibody as a competing protein.[27,32] The antibody exhibits 10 accessible thiol groups, and therefore, we postulated that the antibody would fully displace a pre-adsorbed layer HSA or thiolated HSA analogues with fewer than 10 thiols, if allowed to reach equilibrium. To measure protein exchange rates, HSA, 3T-HSA, and 5T-HSA were added to AuNPs in excess to adsorb at saturating coverage. After the removal of excess HSA or T-HSA analogues, an anti-HRP antibody was introduced to the bioconjugate and incubated for 1−72 h to allow for protein exchange. At defined time points, HRP was added in 30× molar excess and the quantity of HRP captured by the conjugates was normalized to the maximum number of HRP molecules captured by a fully saturated anti-HRP bioconjugate, e.g., positive control conjugate. The number of HRP molecules captured by the bioconjugate after allowing for protein exchange directly correlated with the quantity of displaced HSA or T-HSA. (Figure 5A). The fraction of HSA displaced by anti-HRP IgG ranged from 91−95% at each time point (1−72 h). Greater than 90% of native HSA was displaced from the AuNP conjugate by anti-HRP IgG in less than 1 h, suggesting that the protein adsorbed through a single thiol group rapidly exchanged from the surface. The 3T-HSA analogue also approached 90% desorption after 72 h; however, the desorption rate was slower than that of the native HSA with 53 ± 22, 67 ± 9, and 75 ± 3% desorption after 1, 4, and 9 h, respectively (Figure 5A). The IgG also effectively displaced the 5T-HSA analogue, with nearly 80% of 5T-HSA displaced after 72 h and the data trending toward additional desorption with increased time (Figure 5A). Notably, the protein exchange rate, i.e., HSA desorption rate, inversely correlated with the number of thiol groups accessible on the HSA molecule, provided that the adsorbed HSA had fewer thiol groups than the competing IgG protein. These results establish that IgG adsorption is HSA analogue-dependent, which supports a displacement mechanism, as a co-adsorption mechanism would result in similar co-adsorption for each of the HSA analogues. The 4 h time point is selected to further highlight the fraction of HSA desorbed with respect to the number of thiol groups (Figure 5B). This view of the data can be used to inform

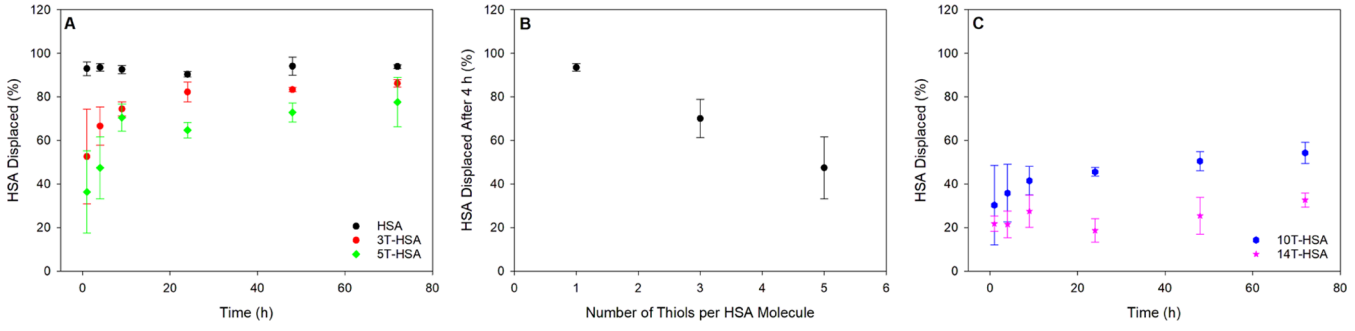

Figure 5. Effect of surface-accessible thiols on the displacement of HSA conjugated to AuNP by a competing antibody in solution. (A) Time course of HSA displacement for HSA and T-HSA analogues with fewer thiol functional groups than the competing protein. (B) Displacement of HSA and T-HSA after 4 h of protein exchange as a function of the number of free thiols on HSA. (C) Time course for the displacement of T-HSA analogues with equivalent or more thiol functional groups than the competing protein.

https://doi.org/10.1021/acs.langmuir.2c03429
Langmuir 2023, 39, 3720−3728

protein design to synthesize bioconjugates with a targeted fraction of protein release in a given time period (4 h in this example).

More extensively modified HSA analogues were also investigated for protein exchange with an anti-HRP IgG antibody (Figure 5C). 10T-HSA was also displaced from the AuNP surface by IgG at a slower rate than the less thiolated HSA analogues; however, after 72 h of allowing the protein to exchange, only 54 ± 5% of the 10T-HSA was displaced. A relatively modest increase in 10T-HSA displacement after the 24 h time point was observed, and given that the two competing proteins in this experiment have an equivalent number of accessible thiols, it is possible that the IgG would not fully displace the 10T-HSA at equilibrium. Figure 5C demonstrates that the 14T-HSA formed a stable and robust adlayer in which the bioconjugate did not display a time-dependent displacement by IgG. Following protein exchange at all time points, the 14T-HSA conjugates produced 22−26% of the antigen-binding activity relative to the fully modified anti-HRP conjugate that served as a positive control. These data are consistent with a previously published result and are attributed to antibody molecules backfilling pinholes in the disordered monolayer on the 14T-HSA bioconjugate rather than displacement of adsorbed 14T-HSA molecules.[29,32,56]

Protein exchange studies were conducted at 37 °C to assess the impact of elevated temperature on desorption/exchange rates and mimic the physiological internal temperature of a healthy human. After allowing 1 h for protein exchange at the elevated temperature, less protein exchange was recorded compared to the same experiment carried out at room temperature (22 °C) (Figure 6). While protein adsorption

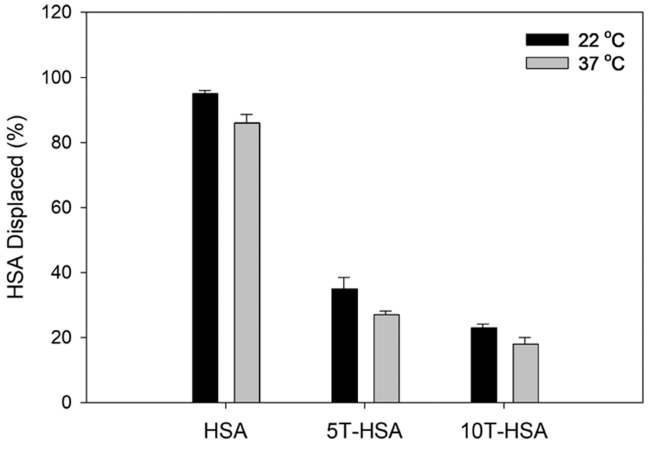

Figure 6. Effect of temperature on the displacement of HSA and T-HSA analogues conjugated to AuNP by a competing antibody in solution.

rate has been shown to increase at elevated temperatures,[12,57−59] these results suggest slower desorption rates at elevated temperatures. Protein exchange on a AuNP surface has been described as an associative exchange mechanism, where the competing protein, e.g., IgG, first adsorbs onto the AuNP surface, followed by the subsequent desorption of the HSA or T-HSA molecule.[29,32] At elevated temperatures, the pre-adsorbed protein is more likely to undergo slight thermal unfolding or exhibit increased flexibility resulting in an increase in contact area with the AuNP.[60] This process results in the less-exposed gold surface for the competing protein to associate with and potentially increases the affinity of the pre-adsorbed HSA molecules because of the increased number of interactions with the AuNP surface. Thus, we conclude that these results are supportive of an associative mechanism of protein exchange.

BSA Desorption from AuNP in Normal Bovine Serum. An anti-HRP antibody as a competing protein is convenient in that it allows for precise control over the environment during protein exchange studies with a AuNP bioconjugate. Moreover, it provides a facile means to quantify protein exchange. However, this model system has less utility in exploring desorption in more complex and realistic environments. Therefore, we developed a fluorescence-based method to quantify protein exchange in a more complex matrix, such as serum. To this end, a fluorescently labeled protein was utilized to synthesize a protein−AuNP bioconjugate and the purified conjugate was introduced into the serum to allow for protein displacement from the AuNP surface by serum proteins. The displaced protein was then determined from the fluorescence intensity acquired from the collected supernatant. Fluorescein isothiocyanate-labeled bovine serum albumin (FITC BSA) was readily available in the requisite quantity and concentration needed to perform the protein exchanges studies; thus, bioconjugates were prepared with FITC BSA and thiolated FITC BSA (FITC T-BSA) analogues rather than fluorescently labeled HSA. It should be noted that BSA has a similar molecular weight, structure, and composition as HSA and is a suitable surrogate (Figures S2 and S3).

A library of FITC-labeled BSA analogues was synthesized by controlling the molar excess of the Traut's reagent to vary the number of installed thiols, and the number of free thiols present in FITC BSA analogues was quantified using Ellman's reagent (Table S1). Fully coated FITC BSA or FITC T-BSA conjugates were prepared, purified to remove excess fluorescently labeled protein, and then dispersed in 10% bovine serum. Following a 24 h incubation period to allow for serum proteins to displace the adsorbed BSA or T-BSA analogues, the AuNP conjugate was centrifuged into a pellet and the supernatant was analyzed via fluorescence to assess the displaced BSA or T-BSA. Serum is a complex mixture of many proteins, including IgG; thus, it was expected that BSA and T-BSA analogues with fewer than 10 thiols would be displaced. As anticipated, Figure 7 shows that BSA desorbs from the AuNP surface when suspended in serum, and the quantity of desorbed protein is inversely related to the number of accessible thiol groups.

■ CONCLUSIONS

Here, we established that the desorption rate of an immobilized protein on a gold nanoparticle is governed by the number of solvent-accessible thiol groups on the protein. Surface-accessible thiols were readily installed on human serum albumin using a simple one-step reaction with Traut's reagent, and the number of installed thiols was quantitatively controlled by varying the molar excess of the chemical modifier. Using this facile method, a library of thiolated HSA analogues was synthesized and adsorbed onto AuNPs to form bioconjugates. We found that greater than 90% of the pre-adsorbed native HSA, containing only one thiol functional group, was displaced in less than 1 h when suspended in solution with a single competing protein, e.g., IgG. The desorption rate was reduced as the number of thiol groups installed on HSA increased. BSA-AuNP bioconjugates were then synthesized and sus-

https://doi.org/10.1021/acs.langmuir.2c03429
Langmuir 2023, 39, 3720−3728

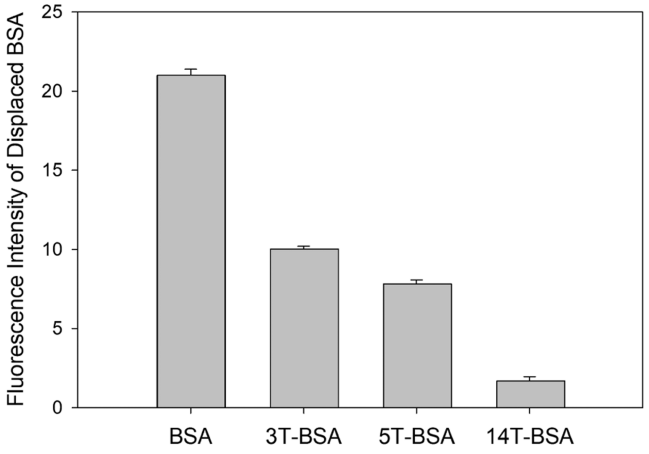

Figure 7. Stability of BSA-AuNP conjugates in normal serum. Desorption of fluorescently labeled BSA and T-BSA analogues from AuNPs after suspension in 10% normal bovine serum for 24 h.

pended in bovine serum, a more complex environment, and a similar trend in desorption rate was observed with respect to protein thiolation. These data are consistent with other works that have identified Au−S interactions as the dominating force responsible for protein adsorption onto AuNP. The methods and findings of this work can easily be adapted to other protein−AuNP conjugate systems to tailor the temporal release of therapeutic protein in a drug delivery application.

■ ASSOCIATED CONTENT

Supporting Information

The Supporting Information is available free of charge at https://pubs.acs.org/doi/10.1021/acs.langmuir.2c03429.

Calibration curve for quantifying thiol concentration, structure of HSA and BSA, solvent accessibility of HSA and BSA amino acids; measured number of thiols on fluorescently labeled BSA (PDF)

■ AUTHOR INFORMATION

Corresponding Author

Jeremy D. Driskell − *Department of Chemistry, Illinois State University, Normal, Illinois 61790, United States;* orcid.org/0000-0001-5082-898X; Email: jdriske@ilstu.edu

Author

Tosin Ogunlusi − *Department of Chemistry, Illinois State University, Normal, Illinois 61790, United States*

Complete contact information is available at: https://pubs.acs.org/10.1021/acs.langmuir.2c03429

Notes

The authors declare no competing financial interest.

■ ACKNOWLEDGMENTS

This work was funded by the National Science Foundation through the Macromolecular, Supramolecular, and Nanochemistry Program, Award # CHE-2203740. Partial support was also provided by Illinois State University.

■ REFERENCES

(1) Tan, Y. F.; Lao, L. L.; Xiong, G. M.; Venkatraman, S. Controlled-Release Nanotherapeutics: State of Translation. *J. Controlled Release* **2018**, *284*, 39−48.
(2) Simonazzi, A.; Cid, A. G.; Villegas, M.; Romero, A. I.; Palma, S. D.; Bermudez, J. M. *Drug Targeting and Stimuli Sensitive Drug Delivery Systems*; Grumezescu, A. M., Ed.; William Andrew Publishing, 2018; pp 81−116.
(3) Karimi, M.; Zangabad, P. S.; Ghasemi, A.; Amiri, M.; Bahrami, M.; Malekzad, H.; Asl, H. G.; Asl, Z.; Bozorgomid, M.; Ghasemi, A.; Boyuk, M. R. R. T.; Hamblin, M. R. Temperature-Responsive Smart Nanocarriers for Delivery of Therapeutic Agents: Applications and Recent Advances. *ACS Appl. Mater. Interfaces* **2016**, *8*, 21107−21133.
(4) Li, J.; Mooney, D. J. Designing Hydrogels for Controlled Drug Delivery. *Nat. Rev. Mater.* **2016**, *1*, No. 16071.
(5) Moerz, S. T.; Huber, P. Protein Adsorption into Mesopores: A Combination of Electrostatic Interaction, Counterion Release, and Van Der Waals Forces. *Langmuir* **2014**, *30*, 2729−2737.
(6) Dawson, J. I.; Kanczler, J. M.; Yang, X. B.; Attard, G. S.; Oreffo, R. O. C. Clay Gels for the Delivery of Regenerative Microenvironments. *Adv. Mater.* **2011**, *23*, 3304−3308.
(7) Gibbs, D. M. R.; Black, C. R. M.; Hulsart-Billstrom, G.; Shi, P.; Scarpa, E.; Oreffo, R. O. C.; Dawson, J. I. Bone Induction at Physiological Doses of Bmp through Localization by Clay Nanoparticle Gels. *Biomaterials* **2016**, *99*, 16−23.
(8) Koshy, S. T.; Zhang, D. K. Y.; Grolman, J. M.; Stafford, A. G.; Mooney, D. J. Injectable Nanocomposite Cryogels for Versatile Protein Drug Delivery. *Acta Biomater.* **2018**, *65*, 36−43.
(9) Adamczyk, Z. Protein Adsorption: A Quest for a Universal Mechanism. *Curr. Opin. Colloid Interface Sci.* **2019**, *41*, 50−65.
(10) Bhakta, S. A.; Evans, E.; Benavidez, T. E.; Garcia, C. D. Protein Adsorption onto Nanomaterials for the Development of Biosensors and Analytical Devices: A Review. *Anal. Chim. Acta* **2015**, *872*, 7−25.
(11) Lynch, I.; Dawson, K. A. Protein-Nanoparticle Interactions. *Nano Today* **2008**, *3*, 40−47.
(12) Rabe, M.; Verdes, D.; Seeger, S. Understanding Protein Adsorption Phenomena at Solid Surfaces. *Adv. Colloid Interface Sci.* **2011**, *162*, 87−106.
(13) Amina, S. J.; Guo, B. A Review on the Synthesis and Functionalization of Gold Nanoparticles as a Drug Delivery Vehicle. *Int. J. Nanomed.* **2020**, *15*, 9823−9857.
(14) Ghosh, P.; Han, G.; De, M.; Kim, C. K.; Rotello, V. M. Gold Nanoparticles in Delivery Applications. *Adv. Drug Delivery Rev.* **2008**, *60*, 1307−1315.
(15) Kong, F. Y.; Zhang, J. W.; Li, R. F.; Wang, Z. X.; Wang, W. J.; Wang, W. Unique Roles of Gold Nanoparticles in Drug Delivery, Targeting and Imaging Applications. *Molecules* **2017**, *22*, No. 1445.
(16) Boisselier, E.; Astruc, D. Gold Nanoparticles in Nanomedicine: Preparations, Imaging, Diagnostics, Therapies and Toxicity. *Chem. Soc. Rev.* **2009**, *38*, 1759−1782.
(17) Curry, T.; Kopelman, R.; Shilo, M.; Popovtzer, R. Multifunctional Theranostic Gold Nanoparticles for Targeted Ct Imaging and Photothermal Therapy. *Contrast Media Mol. Imaging* **2014**, *9*, 53−61.
(18) Huang, H. C.; Barua, S.; Sharma, G.; Dey, S. K.; Rege, K. Inorganic Nanoparticles for Cancer Imaging and Therapy. *J. Controlled Release* **2011**, *155*, 344−357.
(19) Ali, M. R. K.; Wu, Y.; El-Sayed, M. A. Gold-Nanoparticle-Assisted Plasmonic Photothermal Therapy Advances toward Clinical Application. *J. Phys. Chem. C* **2019**, *123*, 15375−15393.
(20) Das, M.; Shim, K. H.; An, S. S. A.; Yi, D. K. Review on Gold Nanoparticles and Their Applications. *Toxicol. Environ. Health Sci.* **2011**, *3*, 193−205.
(21) Dreaden, E. C.; Alkilany, A. M.; Huang, X.; Murphy, C. J.; El-Sayed, M. A. The Golden Age: Gold Nanoparticles for Biomedicine. *Chem. Soc. Rev.* **2012**, *41*, 2740−2779.
(22) Dykman, L.; Khlebtsov, N. Gold Nanoparticles in Biomedical Applications: Recent Advances and Perspectives. *Chem. Soc. Rev.* **2012**, *41*, 2256−2282.

(23) Giljohann, D. A.; Seferos, D. S.; Daniel, W. L.; Massich, M. D.; Patel, P. C.; Mirkin, C. A. Gold Nanoparticles for Biology and Medicine. *Angew. Chem., Int. Ed.* **2010**, *49*, 3280−3294.
(24) Xiao, T.; Qin, J.; Peng, C.; Guo, R.; Lu, X.; Shi, X. A Dendrimer-Based Dual Radiodense Element-Containing Nanoplatform for Targeted Enhanced Tumor Computed Tomography Imaging. *Langmuir* **2020**, *36*, 3096−3103.
(25) Yeh, Y.-C.; Creran, B.; Rotello, V. M. Gold Nanoparticles: Preparation, Properties, and Applications in Bionanotechnology. *Nanoscale* **2012**, *4*, 1871−1880.
(26) Liu, F.; Wang, L.; Wang, H.; Yuan, L.; Li, J.; Brash, J. L.; Chen, H. Modulating the Activity of Protein Conjugated to Gold Nanoparticles by Site-Directed Orientation and Surface Density of Bound Protein. *ACS Appl. Mater. Interfaces* **2015**, *7*, 3717−3724.
(27) Ruiz, G.; Ryan, N.; Rutschke, K.; Awotunde, O.; Driskell, J. D. Antibodies Irreversibly Adsorb to Gold Nanoparticles and Resist Displacement by Common Blood Proteins. *Langmuir* **2019**, *35*, 10601−10609.
(28) Siriwardana, K.; Wang, A.; Vangala, K.; Fitzkee, N.; Zhang, D. Probing the Effects of Cysteine Residues on Protein Adsorption onto Gold Nanoparticles Using Wild-Type and Mutated Gb3 Proteins. *Langmuir* **2013**, *29*, 10990−10996.
(29) Vangala, K.; Ameer, F.; Salomon, G.; Le, V.; Lewis, E.; Yu, L. Y.; Liu, D.; Zhang, D. M. Studying Protein and Gold Nanoparticle Interaction Using Organothiols as Molecular Probes. *J. Phys. Chem. C* **2012**, *116*, 3645−3652.
(30) Wang, A.; Vangala, K.; Vo, T.; Zhang, D.; Fitzkee, N. C. A Three-Step Model for Protein−Gold Nanoparticle Adsorption. *J. Phys. Chem. C* **2014**, *118*, 8134−8142.
(31) Davidson, A. M.; Brust, M.; Cooper, D. L.; Volk, M. Sensitive Analysis of Protein Adsorption to Colloidal Gold by Differential Centrifugal Sedimentation. *Anal. Chem.* **2017**, *89*, 6807−6814.
(32) Awotunde, O.; Okyem, S.; Chikoti, R.; Driskell, J. D. Role of Free Thiol on Protein Adsorption to Gold Nanoparticles. *Langmuir* **2020**, *36*, 9241−9249.
(33) Karimi, M.; Bahrami, S.; Ravari, S. B.; Zangabad, P. S.; Mirshekari, H.; Bozorgomid, M.; Shahreza, S.; Sori, M.; Hamblin, M. R. Albumin Nanostructures as Advanced Drug Delivery Systems. *Expert Opin. Drug Delivery* **2016**, *13*, 1609−1623.
(34) Larsen, M. T.; Kuhlmann, M.; Hvam, M. L.; Howard, K. A. Albumin-Based Drug Delivery: Harnessing, Nature to Cure Disease. *Mol. Cell. Ther.* **2016**, *4*, No. 3.
(35) Wang, S.; Liu, S.; Zhang, Y.; He, J.; Coy, D.; Sun, L. Human Serum Albumin (Hsa) and Its Applications as a Drug Delivery Vehicle. *Health Sci. J.* **2020**, *14*, 1−8.
(36) Micsonai, A.; Bulyáki, É.; Kardos, J. Bestsel: From Secondary Structure Analysis to Protein Fold Prediction by Circular Dichroism Spectroscopy. In *Structural Genomics: General Applications*; Chen, Y. W.; Yiu, C.-P. B., Eds.; Springer U.S.: New York, NY, 2021; pp 175−189.
(37) Micsonai, A.; Wien, F.; Kernya, L.; Lee, Y. H.; Goto, Y.; Refregiers, M.; Kardos, J. Accurate Secondary Structure Prediction and Fold Recognition for Circular Dichroism Spectroscopy. *Proc. Natl. Acad. Sci. U.S.A.* **2015**, *112*, E3095−E3103.
(38) Ruiz, G.; Tripathi, K.; Okyem, S.; Driskell, J. D. Ph Impacts the Orientation of Antibody Adsorbed onto Gold Nanoparticles. *Bioconjugate Chem.* **2019**, *30*, 1182−1191.
(39) Treuel, L.; Brandholt, S.; Maffre, P.; Wiegele, S.; Shang, L.; Nienhaus, G. U. Impact of Protein Modification on the Protein Corona on Nanoparticles and Nanoparticle−Cell Interactions. *ACS Nano* **2014**, *8*, 503−513.
(40) Porollo, A. A.; Adamczak, R.; Meller, J. Polyview: A Flexible Visualization Tool for Structural and Functional Annotations of Proteins. *Bioinformatics* **2004**, *20*, 2460−2462.
(41) Pettersen, E. F.; Goddard, T. D.; Huang, C. C.; Couch, G. S.; Greenblatt, D. M.; Meng, E. C.; Ferrin, T. E. Ucsf Chimera–a Visualization System for Exploratory Research and Analysis. *J. Comput. Chem.* **2004**, *25*, 1605−1612.
(42) He, X. M.; Carter, D. C. Atomic Structure and Chemistry of Human Serum Albumin. *Nature* **1992**, *358*, 209−215.
(43) Chung, W. K.; Russell, B.; Yang, Y.; Handlogten, M.; Hudak, S.; Cao, M.; Wang, J.; Robbins, D.; Ahuja, S.; Zhu, M. Effects of Antibody Disulfide Bond Reduction on Purification Process Performance and Final Drug Substance Stability. *Biotechnol. Bioeng.* **2017**, *114*, 1264−1274.
(44) Dobrovolskaia, M. A.; Patri, A. K.; Zheng, J.; Clogston, J. D.; Ayub, N.; Aggarwal, P.; Neun, B. W.; Hall, J. B.; McNeil, S. E. Interaction of Colloidal Gold Nanoparticles with Human Blood: Effects on Particle Size and Analysis of Plasma Protein Binding Profiles. *Nanomedicine* **2009**, *5*, 106−117.
(45) Hartvig, R. A.; van de Weert, M.; Østergaard, J.; Jorgensen, L.; Jensen, H. Protein Adsorption at Charged Surfaces: The Role of Electrostatic Interactions and Interfacial Charge Regulation. *Langmuir* **2011**, *27*, 2634−2643.
(46) Karyakin, A. A.; Presnova, G. V.; Rubtsova, M. Y.; Egorov, A. M. Oriented Immobilization of Antibodies onto the Gold Surfaces Via Their Native Thiol Groups. *Anal. Chem.* **2000**, *72*, 3805−3811.
(47) Wu, W.-T.; Chen, C.-H.; Chiang, C.-Y.; Chau, L.-K. Effect of Surface Coverage of Gold Nanoparticles on the Refractive Index Sensitivity in Fiber-Optic Nanoplasmonic Sensing. *Sensors* **2018**, *18*, No. 1759.
(48) Bekdemir, A.; Stellacci, F. A Centrifugation-Based Physicochemical Characterization Method for the Interaction between Proteins and Nanoparticles. *Nat. Commun.* **2016**, *7*, No. 13121.
(49) Ke, P. C.; Lin, S.; Parak, W. J.; Davis, T. P.; Caruso, F. A Decade of the Protein Corona. *ACS Nano* **2017**, *11*, 11773−11776.
(50) Shang, L.; Nienhaus, G. U. In Situ Characterization of Protein Adsorption onto Nanoparticles by Fluorescence Correlation Spectroscopy. *Acc. Chem. Res.* **2017**, *50*, 387−395.
(51) Boulos, S. P.; Davis, T. A.; Yang, J. A.; Lohse, S. E.; Alkilany, A. M.; Holland, L. A.; Murphy, C. J. Nanoparticle−Protein Interactions: A Thermodynamic and Kinetic Study of the Adsorption of Bovine Serum Albumin to Gold Nanoparticle Surfaces. *Langmuir* **2013**, *29*, 14984−14996.
(52) Dominguez-Medina, S.; McDonough, S.; Swanglap, P.; Landes, C. F.; Link, S. In Situ Measurement of Bovine Serum Albumin Interaction with Gold Nanospheres. *Langmuir* **2012**, *28*, 9131−9139.
(53) Tsai, D.-H.; DelRio, F. W.; Keene, A. M.; Tyner, K. M.; MacCuspie, R. I.; Cho, T. J.; Zachariah, M. R.; Hackley, V. A. Adsorption and Conformation of Serum Albumin Protein on Gold Nanoparticles Investigated Using Dimensional Measurements and in Situ Spectroscopic Methods. *Langmuir* **2011**, *27*, 2464−2477.
(54) Brewer, S. H.; Glomm, W. R.; Johnson, M. C.; Knag, M. K.; Franzen, S. Probing BSA Binding to Citrate-Coated Gold Nanoparticles and Surfaces. *Langmuir* **2005**, *21*, 9303−9307.
(55) Siriwardana, K.; LaCour, A.; Zhang, D. Critical Sequence Dependence in Multicomponent Ligand Binding to Gold Nanoparticles. *J. Phys. Chem. C* **2016**, *120*, 6900−6905.
(56) Smith, A. M.; Marbella, L. E.; Johnston, K. A.; Hartmann, M. J.; Crawford, S. E.; Kozycz, L. M.; Seferos, D. S.; Millstone, J. E. Quantitative Analysis of Thiolated Ligand Exchange on Gold Nanoparticles Monitored by 1h Nmr Spectroscopy. *Anal. Chem.* **2015**, *87*, 2771−2778.
(57) Lei, M.; Zhang, W.; Yi, C.; Yan, L.; Tian, Y. Zwitterionic Nanogels with Temperature Sensitivity and Redox-Degradability for Controlled Drug Release. *Colloids Surf., B* **2021**, *206*, No. 111959.
(58) Stetsyshyn, Y.; Raczkowska, J.; Lishchynskyi, O.; Bernasik, A.; Kostruba, A.; Harhay, K.; Ohar, H.; Marzec, M. M.; Budkowski, A. Temperature-Controlled Three-Stage Switching of Wetting, Morphology, and Protein Adsorption. *ACS Appl. Mater. Interfaces* **2017**, *9*, 12035−12045.
(59) Wang, S.; Ou, X.; Yi, M.; Li, J. Spontaneous Desorption of Protein from Self-Assembled Monolayer (Sam)-Coated Gold Nanoparticles Induced by High Temperature. *Phys. Chem. Chem. Phys.* **2022**, *24*, 2363−2370.
(60) Fang, H. W.; Hsieh, M. C.; Huang, H. T.; Tsai, C. Y.; Chang, M. H. Conformational and Adsorptive Characteristics of Albumin

https://doi.org/10.1021/acs.langmuir.2c03429
Langmuir 2023, 39, 3720−3728

Affect Interfacial Protein Boundary Lubrication: From Experimental to Molecular Dynamics Simulation Approaches. *Colloids Surf., B* **2009**, *68*, 171−177.

https://doi.org/10.1021/acs.langmuir.2c03429
Langmuir 2023, 39, 3720−3728